Acta Oceanol. Sin., 2017, Vol. 36, No. 7, P. 66–76
DOI: 10.1007/s13131-017-1085-0
http://www.hyxb.org.cn
E-mail: hyxbe@263.net

Use of portable X-ray fluorescence in the analysis of surficial sediments in the exploration of hydrothermal vents on the Southwest Indian Ridge

LIAO Shili[1, 2, 3], TAO Chunhui[1, 2*], LI Huaiming[1, 2], ZHANG Guoyin[1, 2], LIANG Jin[1, 2], YANG Weifang[1, 2]

[1] Second Institute of Oceanography, State Oceanic Administration, Hangzhou 310012, China

[2] Key Laboratory of Submarine Geosciences, State Oceanic Administration, Hangzhou 310012, China

[3] Key Laboratory of Marine Mineral Resources, Ministry of Land and Resources, Guangzhou 510075, China

Received 5 May 2016; accepted 17 March 2017

Abstract

Hydrothermal plumes released from the eruption of sea floor hydrothermal fluids contain large amounts of ore-forming materials. They precipitate within certain distances from the hydrothermal vent. Six surficial sediment samples from the Southwest Indian Ridge (SWIR) were analyzed by a portable X-ray fluorescence (PXRF) analyzer on board to find a favorable method fast and efficient enough for sea floor sulfide sediment geochemical exploration. These sediments were sampled near, at a moderate distance from, or far away from hydrothermal vents. The results demonstrate that the PXRF is effective in determining the enrichment characteristics of the ore-forming elements in the calcareous sediments from the mid-ocean ridge. Sediment samples (>40 mesh) have high levels of elemental copper, zinc, iron, and manganese, and levels of these elements in sediments finer than 40 mesh are lower and relatively stable. This may be due to relatively high levels of basalt debris/glass in the coarse sediments, which are consistent with the results obtained by microscopic observation. The results also show clear zoning of elements copper, zinc, arsenic, iron, and manganese in the surficial sediments around the hydrothermal vent. Sediments near the vent show relatively high content of the ore-forming elements and either high ratios of copper to iron content and zinc to iron content or high ratios of copper to manganese content and zinc to manganese content. These findings show that the content of the ore-forming elements in the sediments around hydrothermal vents are mainly influenced by the distance of sediments to the vent, rather than grain size. In this way, the PXRF analysis of surface sediment geochemistry is found to satisfy the requirements of recognition geochemical anomaly in mid-ocean ridge sediments. Sediments with diameters finer than 40 mesh should be used as analytical samples in the geochemical exploration for hydrothermal vents on mid-oceanic ridges. The results concerning copper, zinc, arsenic, iron, and manganese and their ratio features can be used as indicators in sediment geochemical exploration of seafloor sulfides.

Key words: mid-ocean ridge sediments, hydrothermal activity, portable X-ray fluorescence, geochemical exploration

Citation: Liao Shili, Tao Chunhui, Li Huaiming, Zhang Guoyin, Liang Jin, Yang Weifang. 2017. Use of portable X-ray fluorescence in the analysis of surficial sediments in the exploration of hydrothermal vents on the Southwest Indian Ridge. Acta Oceanologica Sinica, 36(7): 66–76, doi: 10.1007/s13131-017-1085-0

1 Introduction

Sea floor polymetallic sulfides have high levels of the elements Cu, Zn, Au, and Ag, and, under certain geological conditions, massive ore deposits with a size of million tons can be formed (Hannington et al., 2011; Herzig and Hannington, 1995). As a result, these potential resources have become highly valued by countries all over the world. However, because it is a very new field, prospecting for the seafloor polymetallic sulfides lacks well-developed theoretical bases and standard methods of investigation and prospecting. As shown in earlier work, the hydrothermal plumes formed by the eruption of the seafloor hydrothermal fluids are rich in ore-forming elements (German and Sparks, 1993). Although some of the larger particles dispersed within several hundred meters of the vent, more than 90% of these materials were found to precipitate far away from the vent during the plume drifting and dispersing (Feely et al., 1992; Rona, 1984). After hydrothermal activity ceased, even though the sediments were oxidized, the recorded ore-forming information in the sediments were reserved (Feely et al., 1987). Therefore, the geochemical features of the deep-sea sediments might be suitable indicators of geochemical exploration (Marchig et al., 1982). However, though there have been many studies of deep-sea sediments, most of them were focused on mineral composition, sources, and the sediment environment (Graham et al., 1997; Meinhardt et al., 2014; Palma et al., 2013). Studies of hydrothermal sediments have usually concentrated on the geochemical and mineralogical characteristics of metalliferous sediments such as pollymetallic ooze and collapsed chimneys (German et al., 1993; Rusakov et

Foundation item: The Open Fund of Key Laboratory of Marine Mineral Resources, Ministry of Land and Resources under contract No. KLMMR-2015-B-03; the China Ocean Mineral Resources Research and Development Association Project under contract Nos DY125-11-R-01 and DY125-11-R-05; the National Basic Research Program (973 program) of China under contract No. 2012CB417305.
*Corresponding author, E-mail: taochunhuimail@163.com

al., 2013). Only a few studies of the geochemical exploration of sediments have been reported (German, 2003; Yang et al., 2011). Marchig et al. (1982) established geochemical indicators that differentiate hydrothermal sediments and non-hydrothermal sediments. Cronan (1983) distinguished two sediment types formed on different settings in the western Pacific using sedimentary geochemistry and identified various potential prospecting areas of polymetallic sulfides. Shearme et al. (1983) compared sediment geochemical anomaly features near two hydrothermal vents in the trans-Atlantic-geotraverse (TAG) hydrothermal field. Lisitzin et al. (1997) analyzed geochemical halo characteristics of sediments at mid-oceanic ridges of different spreading rates and pointed out that geochemical halo of the hydrothermal vent located on slow-spreading mid-oceanic ridge was normally restricted in the rift valleys and rarely spread out of the rift valley. Wang et al. (2014) preliminarily estimated the influence range of hydrothermal activities in the 49.6°E hydrothermal field on the Southwest Indian Ridge (SWIR) using the ratio of sum of the content of aluminum, iron and manganese to the content of aluminum. Russian researchers have also used sedimentary geochemistry to evaluate massive seafloor sulfides in their contract zone on the North Mid-Atlantic Ridge. However, no related papers have been published.

Owing to the huge cost of the off-shore exploration, in the studies cited above, all samples were collected from the ocean and brought back to labs for analysis, which is time consuming, expensive, and exposes the samples to danger of pollution during the storage and transportation processes, thus affecting the reliability of the measured results. Some way of collecting as much ore-prospecting information as possible, identifying anomalies quickly and effectively, and evaluating and verifying anomalies on board the ship would reduce the randomness of the investigation and sampling processes and the costs of exploration considerably. This is one of the challenges currently facing polymetallic sulfide exploration. Portable X-ray fluorescence (PXRF) analyzers can assess multi-element content rapidly *in situ*, in a semi-quantitative manner. Because PXRF equipment is convenient to carry, and it does not require complex acid digestion before analysis, direct and quick analysis of vast powders or solid samples can be realized in field. For these reasons, the PXRF is already widely used in the artworks, archaeology, alloy analysis, and environmental studies (Melquiades and Appoloni, 2004; Piorek, 1997). Recently, with the development of science and technology, both the detection limit and precision of the PXRF have been improved considerably (Hou et al., 2004; Kenna et al., 2011). Some researchers have started using the PXRF in ore exploration (Fisher et al., 2014) and made great progress, such as identifying regional elements distribution characteristics, differentiation in volcanic facies, and evaluation mineralogical and elemental distribution features of drill cores (Arne et al., 2014; Yuan et al., 2014; Xia et al., 2011). To date, the PXRF has attracted attention both home and abroad in using in ore exploration. The international journal *Geochemistry: Exploration, Environment, Analysis* published a special issue concerning the PXRF in the 2014. The most recent findings, such as the evaluation of factors that influence PXRF tests (Hall et al., 2014), correction methods (Piercey and Devine, 2014), and applications of the PXRF in exploration for gold, copper, zinc, and nickel ores (Arne et al., 2014; Gazley et al., 2014; Ross et al., 2014) have been reported. In this paper, the PXRF analyzer was used to evaluate surficial sediments collected from the middle portion of a polymetallic sulfide contract zone allocated to China, and the contents of specific elements in sediments of different grain sizes were compared. These results could be useful on sampling methods and prospecting effects of using sedimentary geochemical exploration for hydrothermal vents.

2 Geological setting

The SWIR is the main border between the African and Antarctic plates. It extends around 8 000 km from the Bouvet triple junction (BTJ) in the west to the Rodrigues triple junction (RTJ) in the east. The SWIR is classified as an ultra-slow spreading mid-oceanic ridge with a semi-spreading rate around 0.7–0.9 cm/a (Dick et al., 2003). This ridge is characterized by very rugged topography and an axial rift valley with water depths deeper than 5 000 m, and it is cut by a series of north-south transform faults (Fig. 1). Influenced by the Marion hotspot on the southwest, this region shows strong negative residual mantle Bouguer gravity

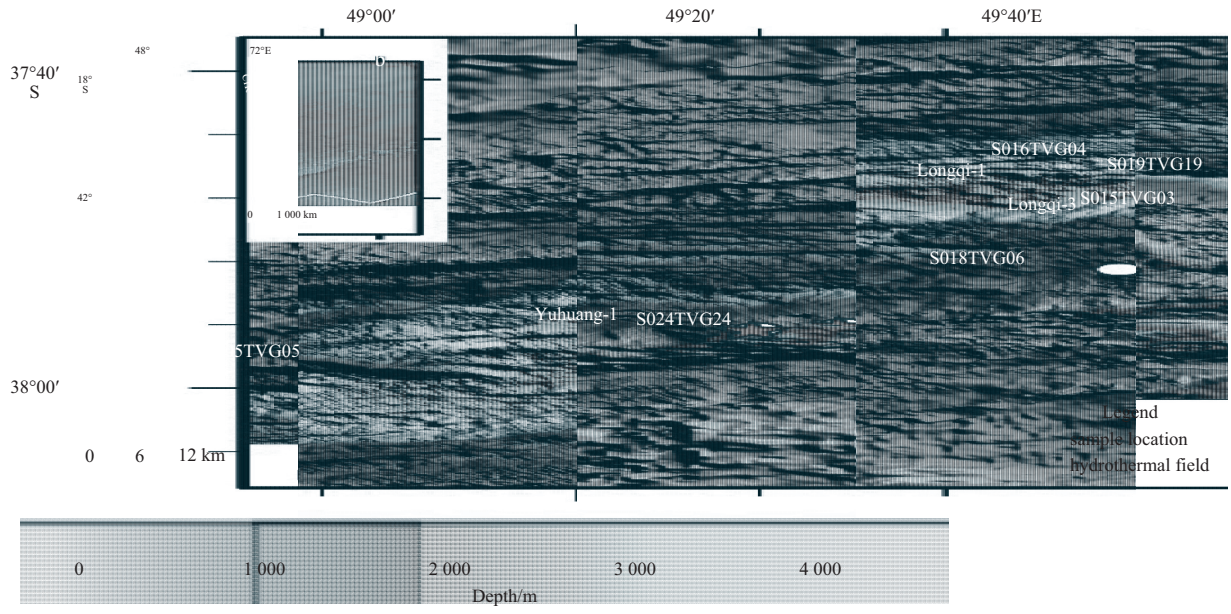

Fig. 1. Location and topography of the study area. The white points show the sampling position.

anomalies, indicating relatively active crust-mantle exchange and deep magmatism in this region, as well as sufficient supply of lava and heat (Georgen et al., 2001; Sauter et al., 2001, 2009; Wang et al., 2013). These conditions are sufficient for the occurrence of sea floor hydrothermal activity and the formation of sulfide deposits.

The study area is located in the middle of the polymetallic sulfide exploration contract zone of China (at the SWIR), between the Indomed and Gallieni transform faults. The axis of this segment strikes NEE with rugged terrain, and the water depth varies from 1 500 to 4 000 m. The central rift valley of this segment is well developed, where the water is relatively deep on the northern side of its axis and relatively shallow on the southern side (Fig. 1). The results of the investigation showed that the lowest layer of water mainly flow to the west with intensive mixture features and a maximum velocity of 20–30 cm/s (Liao et al., 2016). Previous surveys indicated that basalt is widely exposed in this region, but gabbro, diabase, and serpentinized peridotite were also found in some areas (Zhou and Dick, 2013; Han et al., 2012). In this region, modern sediment precipitation is rare, mainly distributed in the rift valley of the mid-oceanic ridge. They consist mainly of calcareous nannofossil and foraminifera, with minor clay minerals, indicating that they are typical pelagic sediments (Li et al., 2016; Chen et al., 2013). To date, three hydrothermal areas have been discovered in this region: Longqi-1, Yuhuang-1, and Longqi-3, among which, the Longqi-1 hydrothermal field is the first active field found on the ultra-slow spreading mid-oceanic ridge in 2007 (Tao et al., 2012, 2014). It mainly consists of chalcopyrite, pyrite, and sphalerite, similar to that of the sulfide chimneys found in the East Pacific Rise and the Mid-Atlantic Ridge (Tao et al., 2011). The survey of *Jiaolong* showed there to be various types of hydrothermal vents with different temperatures. The Yuhuang-1 hydrothermal field is located on the south rift wall of the rift valley with water depth between 1 400 and 1 600 m. It is the shallowest hydrothermal field yet to be discovered at the Southwest Indian Ocean Ridge (Han et al., 2010). The topographic features, mineral composition, trace elements, and sulfur isotopic characteristics indicate that the formation of the Yuhuang-1 hydrothermal field probably contributed to volcanic activity.

3 Sample collection and analytic methods

3.1 *Sample collection*

The sediment samples were collected by the 34th cruise of R/V *Dayang Yihao* near the Longqi-1 hydrothermal field on the Southwest Indian Ocean Ridge in 2015. Samples were collected by television grab (TVG) with water depth between 1 494 and 3 090 m, which is lower than the calcite compensation depth (CCD) in this area. In order to compare geochemical characteristics of the sediments from different distances to the hydrothermal activity field, six samples were collected from close to the hydrothermal field, a moderate distance from the hydrothermal field, and far from the hydrothermal field. The samples obtained far from the hydrothermal field were representative of the background sediments. The majority of the samples far from the hydrothermal field consisted of foraminifera sand with minor volcanic glass or clastic basalt. However, a few other samples mainly consisted of calcareous ooze. Sampling locations and descriptions are shown in Table 1.

3.2 *Analytical instruments and methods*

3.2.1 *Mineral analysis*

Sediments were observed using a Dino-lite AM4113T handheld USB microscope that has two magnification ratios: 20X–50X and 200X.

3.2.2 *PXRF analysis*

The sediments were analyzed on board the ship using a XL3t-950 portable XRF (PXRF) manufactured by the Thermo Fisher Scientific Inc. Because the sediments in the mid-oceanic ridges mainly consist of calcareous foraminifera sand or calcareous ooze, and the objects investigated in this study were polymetallic sulfides, a test-all mode was used to analyze the contents of elements of Cu, Zn, As, Fe, Mn, S, Ca, Si and Sr. The analyzing results of these elements are given in 10^{-6} (μg/g) level. Before analysis, the samples were dried to reduce the influence of humidity on the test results (Arne et al., 2014). Because the 4.0 μm prolene thin films showed the most pronounced light transmittance, stain-resistance, and strength (Hall et al., 2014), the 4 μm-polypropylene thin films provided by Premier were used in this study. During analysis, the test time was set to 60 s in order to determine contents of most elements accurately (Piercey and Devine, 2014). An average forward mode (the average of *N* times of recent results would be calculated automatically) was used, in which the average test number was set to 3 in order to reduce the influence of the heterogeneity of the particles in sediment samples. Before testing, the accuracy and stability of the instrument were assessed, and during testing, a standard sample RM180-646 was used to do calibration every time two samples finished their tests.

During analysis, samples with nine different grain size ranges (>20, 20–40, 40–60, 60–80, 80–100, 100–120, 120–160, 160–200, <200 mesh) were tested separately in order to determine the best grain size for use in sediment geochemical exploration for seafloor sulfides. Owing to the fact that contents of elements of Cu and Zn are relatively high in the clay minerals, samples with a grain size coarser than 200 mesh were first elutriated in the distilled water to eliminate the influence of clay minerals attached to the surface of the rock debris or sand. Then these samples were dried and sieved using a nest of standard sieves consisting of 20, 40, 60, 80, 100, 120, 160, and 200 mesh. Samples with a grain size finer than 200 mesh were obtained by dried unelutriated sediments to prevent loss of clay minerals during the elutriation process.

Table 1. Sample positions and descriptions

Sample	South latitude/(°)	East longitude/(°)	Depth/m	Description	Distance to closest hydrothermal field/km	Hydrothermal field
S024TVG24	37.937 58	49.266 24	1 494	grey foraminifera sand	0.18	Yuhuang-1
S015TVG03	37.786 32	49.731 43	2 230	pale yellow foraminifera sand	0.20	Longqi-3
S016TVG04	37.768 65	49.702 65	3 090	pale yellow foraminifera sand	3.20	Longqi-3
					4.90	Longqi-1
S019TVG19	37.776 63	49.764 34	3 051	grey foraminifera sand	3.06	Longqi-3
S005TVG05	37.976 73	48.824 11	2 306	grey foraminifera sand	38.94	Yuhuang-1
S018TVG06	37.874 76	49.579 23	2 601	pale yellow foraminifera sand	11.94	Longqi-1

4 Analysis of results

4.1 *Mineral characteristics*

Because the constituents of sediments from the mid-ocean ridges were similar to each other, sediment samples collected near the Longqi-1 hydrothermal field were chosen for observation by microscope and considered representative of mid-ocean ridge sediment features (Fig. 2). The results show that sediments coarser than 20 mesh consist mainly of rock debris and basaltic glass (>90%) with minor foraminifera sand and corallum, which indicated that their source was mainly volcanic rocks. Serpentine, mica, asbestos, and chlorite are common in these debris, which may indicate a hydrothermal process. Sulfides that were oxidized to azurite by the sea water were also observed on the surface of some basaltic glass samples, indicating the possibility of hydrothermal activity nearby. Sediment samples of 20–40 mesh also mainly consisted of rock debris and basaltic glass (80%–90%). However, there was more foraminifera sand than in coarser sediments and the grain size of foraminifera sand was large, and there were some dark colored sediments inside the foraminifera sand. For sediments of 40–60 mesh, the content of the foraminifera sand was over 80%, and the rock debris and basaltic glass were no longer major constituents. The mineral composition of the sediments finer than 60 mesh were similar to those of 40–60 mesh size. Sediment samples finer than 200 mesh were also principally made up of foraminifera sand, but there were also a few clay minerals. Overall, the components of the sediments were similar to those of other ridges, which were representative of typical pelagic sediments.

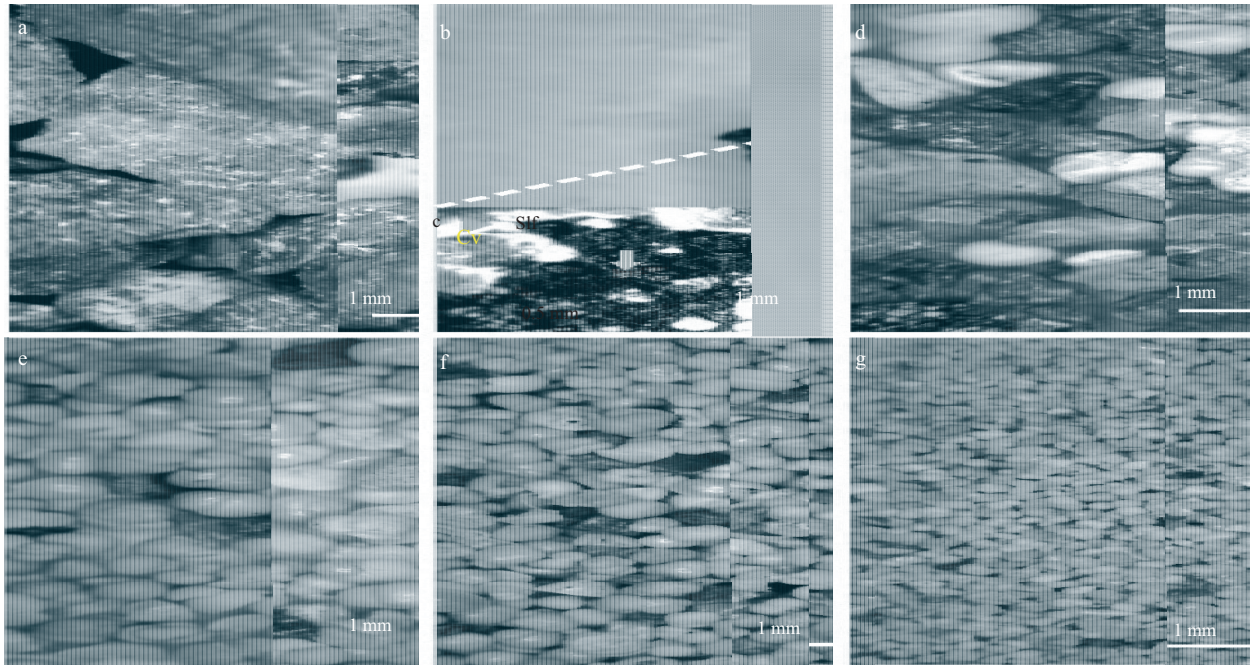

Fig. 2. Photos of different grain size sediment samples. a. Sediment (>20 mesh); b and c. basaltic glass containing metallic sulfides in the sediment (>20 mesh), in particular, c is a locally magnifying image indicating that the sulfides were oxidized to covellite; d. sediments of 20–40 mesh, containing a large amount of basaltic debris and glass but also a large amount of foraminifera sand; e. sediments of 40–60 mesh, mainly containing foraminifera sand, but also few basaltic debris; f. the image of the sediments (60–80 mesh), these sediments show similar composition, mainly a large amount of foraminifera sand and small amount of basaltic debris and glass; and g. sediments of 120–160 mesh, these sediments have similar mineral composition to sediments of 60–80 mesh. Cv represents covellite and Slf sulfide.

4.2 *Results of PXRF analysis and data evaluation*

4.2.1 *Ability of PXRF to detect deep-sea sediment*

Six sediments of varying grain sizes from different stations were analyzed using the PXRF (Table 2). The results show the contents of calcium, silicon, aluminum, copper, zinc, iron, manganese, strontium, zirconium, titanium, sulfur, molybdenum, and arsenic are relatively high and that they can be determined effectively. Among these elements, copper and zinc contents were as high as 823×10^{-6} and 191×10^{-6}, respectively, similar to the features of sediments near hydrothermal vents in other regions. Contents of nickel, arsenic, molybdenum, and niobium varied considerably, with the lowest content below the detection limit. Contents of wolfram, tin, bismuth, lead, mercury, gold, silver, cobalt, chromium, and vanadium were usually below the detection limit. This result was similar to the results reported by Hall et al. (2014) and Mäkinen et al. (2006). Among the major constituents, the contents of aluminum and silicon are usually below 3%, while the highest content of calcium was found to exceed 40%, similar to the results reported by of Huang et al. (2016). Generally, the content of aluminum in the abyssal sediments was attributable to debris component of the sediments. Thus, the results indicated that these samples mainly contained calcium with a few debris derived from base rocks, which shows typical pelagic sediment features. For element content above the detection limit, the results of analysis of strontium, calcium, silicon, iron, manganese, and sulfur contents were very good with relative errors less than 10%. Besides, the analytical errors of the elements copper, zinc, titanium and potassium were between 10%–20%. For elements of molybdenum, arsenic, aluminum, vanadium, titanium, chromi-

Table 2. Seafloor sediment analysis results by PXRF

	Results of analysis						Error /%				
	N	<LOD	Min	Max	Average	SD	Min	Max	Average	SD	Detection
Cu	52	1	11	823	189	17.5	0	65.1	16.8	17.5	detected perfectly, error under 20%
Zn	53	0	18	191	59	5.8	5.2	24.4	12.5	5.8	
Fe	53	0	0.13	10.98	2.65	0.6	0.5	2.6	1.1	0.6	
Mn	53	0	158	23 057	1 398	3.7	1	18.6	7.5	3.7	
Ti	50	3	102	5 669	898	12.5	1.6	49.2	16.1	12.5	
S	53	0	403	3 262	1 097	1.5	2.9	11	7.1	1.5	
Zr	51	2	5	97	16	0.1	0	0.5	0.3	0.1	
Sr	53	0	51	1 328	873	0.5	0.5	3.2	0.9	0.5	
Ca	53	0	37.11	48.44	36.73	0.3	0.3	1.7	0.5	0.3	
K	53	0	331	5 079	1 153	1 018.2	3.1	28.4	13.5	6	
Si	53	0	0.42	17.91	4.77	5.02	0.6	7.9	2.9	1.9	
Ni	46	7	27	622	119	130.7	3.7	57.7	25.6	15.8	most samples detected, average error 20%–50%
As	45	8	3	55	7	8.1	11.6	64.9	38.9	14.3	
Mo	48	5	2	13	5	1.9	12.3	66.4	35.8	13.3	
Nb	50	3	2	11	3	1.3	10.4	63.3	35.1	9.7	
Al	53	0	0.11	2.83	0.68	0.66	2.7	63.5	22.4	16.3	
Rb	50	3	2	13	5	2.9	10.3	54.7	29	10.9	
P	3	50	347	814	607	238.2	16.9	30.5	21.6	20.9	most samples cannot be detected, with average error more than 50%
Au	9	44	4	5	5	0.3	0.5	0.7	0.6	0.1	
Hg	9	44	5	10	8	1.4	0.5	0.7	0.6	0.1	
Co	13	40	40	183	80	38.7	1.5	2.5	1.8	0.3	
Mg	22	31	0.49	3.22	1.31	0.78	6.7	66.4	30.6	1730.2	
Cr	31	22	22	813	225	190.3	2.4	61.9	17.2	16.2	
V	34	19	41	313	105	67.1	10.7	65.3	30.8	14.8	
Pb	35	18	3	132	10	21.7	5.1	62.2	42.5	12.7	
Ba	42	11	53	421	156	74.2	7.4	51.7	22.1	10.1	

Note: Ca, Si, Al, Mg and Fe contents are given in percent, and other elements are in 10^{-6}; *N* represents sample numbers; <LOD means lower than detective limits.

um, and lead, the analytical errors were larger, mostly above 20%. Overall, the analytical error of an element is related to its concentration in the sample. The higher the concentration, the more easily it can be detected and the smaller the test errors. This is similar to test results reported by Wu et al. (2012).

4.2.2 *Data accuracy*

In order to assess the accuracy of the results of the PXRF analysis of abyssal calcareous sediments, the results were compared to the data of the same samples analyzed by an ICP-MS at ALS Laboratory Group in Guangzhou, China. During the ICP-MS measurement, a standard sample was used and 10% repeat samples were inserted to monitor the quality of the data. The test error of the data was found within 5%. During the comparison, the PXRF data for a certain element was plotted on the *x*-axis, the corresponding result obtained by the ICP-MS was plotted on the y-axis, and a linear fit of data to the line y=ax+b was determined. The slope *a* of the linear line represented the degree of deviation of the data. When the slope exceeded 1, the PXRF data were below the true value, and vice versa. R^2 represented the fitting degree of the data. The closer it was to 1, the better the fit. The results show that the slopes for elements Cu, Zn, Ni, Al, and Ti are all above 1 (Fig. 3), indicating that the analytical results of the PXRF were smaller than those measured by the ICP-MS, in particular, the slope for the element Al was close to 3, which indicated that the analytical PXRF value of Al was far below the value indicated by the ICP-MS measurement. The slopes for elements Fe, Mn, and Ca were all smaller than 1, which meant their analytical PXRF values were larger than the values given by the ICP-MS. The fitting degree of the data of elements Zn, Fe, Ni, Al, Ti, and Ca were all above 0.9, and elements of Cu and Mn were above 0.8, which meant the PXRF results for these elements were similar to the results produced in the laboratory. The fitting degree of the data of the element S was below 0.5, which meant the results of XRF measurement were unrelated to the experimental value produced in the laboratory (using the ICP-MS) and was therefore unreliable. Generally speaking, during geochemical exploration, instead of the absolute contents of the elements, geologists care much more about the anomaly area than the background area (Arne et al., 2014). In this way, though PXRF test results were either larger or smaller than the values measured using the ICP-MS. The identification of anomalies is not influenced by these errors as long as all the tests are performed under the same conditions. As a result, the data obtained from the PXRF test for sediments can be applied to the geochemical exploration of hydrothermal vents.

4.2.3 *Assessment of data precision*

The control reference material (CRM) 180-646, which was provided by Thermo Fisher Scientific Inc., was analyzed to assess the stability and precision of the results of the PXRF. We analyzed the same position of CRM 180-646 68 times for this assessment (Table 3). The parameter *Cv* was used to assess the precision of the analysis of the PXRF. This parameter was calculated using the following formula:

$$Cv = (1 - S/\bar{X}) \times 100\%,$$

where *Cv*, *S*, and $\bar{X}$ are precision, standard deviation, and aver-

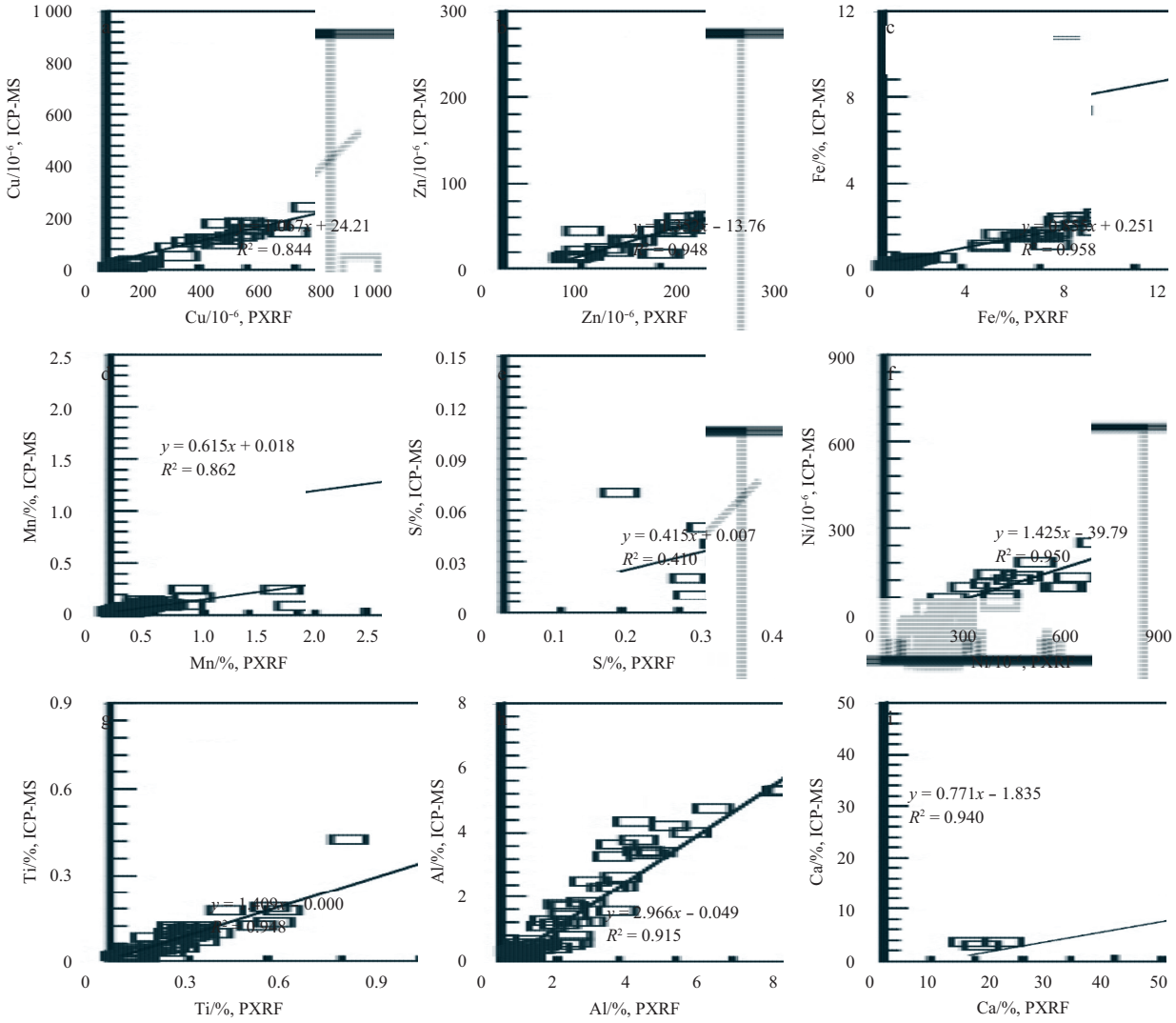

Fig. 3. Comparison of the analytical results produced by PXRF and ICP-MS.

age, respectively. The results show that the precision of analysis of most of the elements is above 95% and that of W, V, Ni, Ca, and Sn is above 80%, indicating that the results of these elements are quite stable and precise. However, the results of Rb were below 60%, indicating that these data should be considered with care.

4.2.4 *Elements combination*

Cluster analysis was used to illustrate the combined features of the elements in these sediments. Before analyzing, the centered log ratio (clr) transformation is applied to process the sediment data (Aitchison, 1986). The cluster analysis was carried out on STATISTICS using 1-Pearson distance measurement and complete linkage. The results show that elements of abyssal calcareous sediments can be divided into two groups (Fig. 4). (1) Fe-Al-Si-Ti-Ni-Mn-Zr can be further divided into two subgroups, Fe-Al-Si-Ti-Ni and Mn-Zr. These elements are the main diagenetic elements, and they may represent the presence of basalt debris in the sediments; and (2) Cu-Zn-As-Ca-Sr can also be further divided into two subgroups, Cu-Zn-As and Ca-Sr. The first subgroup elements are the main ore-forming elements of mid-oceanic ridge seabed massive sulfide. Their close correlation demonstrated that the composition of the sediments had been changed by hydrothermal activity, indicating that these elements could be used in sediment geochemical exploration for hydrothermal activities. The latter subgroup elements probably represent the main calcareous composition of the sediments. These results indicate that the analytical results produced by the PXRF represent the composition of the sediments closely.

5 Discussion

5.1 *Geochemical properties of sediments with different grain sizes*

The chemical composition of the sediments of different grain sizes collected from the same sampling station were compared (Fig. 5). The results demonstrated that, as grain size decreased, the content of Ca gradually increased, stabilizing around 40% for samples finer than 40 mesh. However, the trends of changes in content were just the opposite for Si, Al, and Ti. They showed overall negative correlations between the element concentration and grain size. As shown in earlier studies, Al and Ti mainly represent component of debris in sediments (Bloemsma et al., 2012). Microscopic observation confirmed that coarse samples consisted mainly of debris, but the samples with finer grain sizes consisted primarily of foraminifera sand. In this way, the element characteristics outlined above indicate the composition of the sediments.

Table 3. Analysis of CRM 180-646

	Unit	Number	Min	Max	Average	SD	*Cv*/%
Fe	%	68	4.06	4.23	4.16	0.04	99.10
Sr	10^{-6}	68	108	115	112	1.37	98.78
K	%	68	2.32	2.46	2.39	0.03	98.77
Zr	10^{-6}	68	370	397	385	5.41	98.59
Si	%	68	32.36	34.71	33.70	0.67	98.00
As	10^{-6}	68	97	107	102	2.21	97.84
Th	10^{-6}	68	45	50	47	1.25	97.34
Cu	10^{-6}	68	210	238	225	6.17	97.26
S	%	68	0.16	0.18	0.17	0.01	96.68
Bi	10^{-6}	68	52	61	57	1.90	96.64
Nb	10^{-6}	68	14	17	15	0.56	96.33
Pb	10^{-6}	68	45	55	51	1.92	96.20
Mn	10^{-6}	68	391	475	439	18.45	95.79
Al	%	68	4.19	4.89	4.60	0.19	95.78
Zn	10^{-6}	68	60	75	67	3.08	95.38
Ba	10^{-6}	68	350	449	399	19.10	95.21
Mo	10^{-6}	68	18	23	20	1.15	94.37
P	%	68	0.15	0.20	0.17	0.01	94.28
Ti	%	68	0.42	0.53	0.48	0.03	92.75
Cr	10^{-6}	68	45	161	130	12.42	90.46
W	10^{-6}	68	147	296	185	23.28	87.41
V	10^{-6}	68	97	173	133	17.44	86.86
Ni	10^{-6}	68	37	76	54	7.20	86.72
Ca	%	68	0.75	1.30	0.97	0.14	85.75
Sn	10^{-6}	66	11	23	16	3.09	80.59
Rb	10^{-6}	68	63	151	81	33.16	59.14

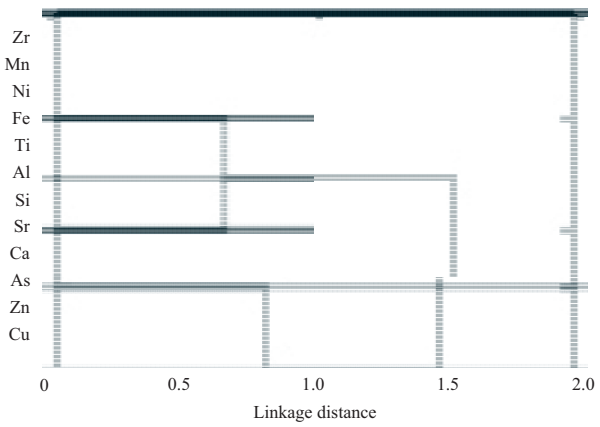

Fig. 4. Cluster analysis of the results of sediments analyzed by the PXRF.

In the two sample stations close to the vent, contents of Cu and Zn are above 400×10^{-6} and 150×10^{-6}, respectively, for those with grain size coarser than 20 and 20–40 mesh. For samples with grain size of 40–60 mesh, contents of Cu and Zn decreased dramatically, to 200×10^{-6} and 50×10^{-6}, respectively, and then stabilized in samples of finer grain sizes. For sample stations located moderate distances from and far from hydrothermal vents, contents of Cu and Zn were relatively low, and the effect of grain size on element content was less pronounced than that of sample stations close to the vent. The features of Fe and Mn were similar to those of Cu and Zn, with high content in samples coarser than 40 mesh, and turn out to be quite stable for samples finer than 40 mesh. For samples with grain size coarser than 20 mesh and within 20–40 mesh from the two samples stations far to the vent, the contents of Fe and Mn were relatively high, similar to samples close to the vent. Microscope observation indicated that basaltic debris and glass were common in samples coarser than 40 mesh, but samples finer than 40 mesh consisted primarily of calcareous foraminifera sand. Previous works have shown the Cu contents to be mainly about 80×10^{-6} in basalts from Mid-Atlantic Ridge (Keays and Scott, 1976). In basalts from the Southwest Indian Ridge, the Cu contents are mainly within 80×10^{-6}–110×10^{-6}, the Fe contents are typically around 7%, and $1\,000\times10^{-6}$–$2\,000\times10^{-6}$ for Mn (Nakamura et al., 2007; Han et al., 2012). Thus, the high levels of ore-forming elements in coarse samples are probably attributable to basaltic debris and glass. Further, the two coarse samples close to the vent, which had significantly high contents of Cu and Zn may be explained by the existence of disseminated mineralization in the basalt debris and the glass (Fig. 2c). Among element ratios, Cu/Fe and Zn/Fe showed an increasing trend with decreases in grain sizes, which means Fe was more concentrated in coarser samples. However, the Fe/Mn ratios in the samples were scattered, without any apparent trend.

Overall, except for somewhat high contents of Cu, Zn, and Fe, element contents of sediments with different grain sizes from the same sampling stations were basically distributed within certain range, showing only trivial variation, which indicates that main factor controlling element contents of the deep-sea sediments is the distance to hydrothermal vent, not grain size. The results also show that the chemical characteristics of the sediments coarser than 40 mesh are significantly influenced by debris, so sediments finer than 40 mesh should be selected to represent geochemical characteristics of sediment samples.

5.2 *Use of indicators in sediment geochemical exploration*

According to the microscopic observation and PXRF analysis

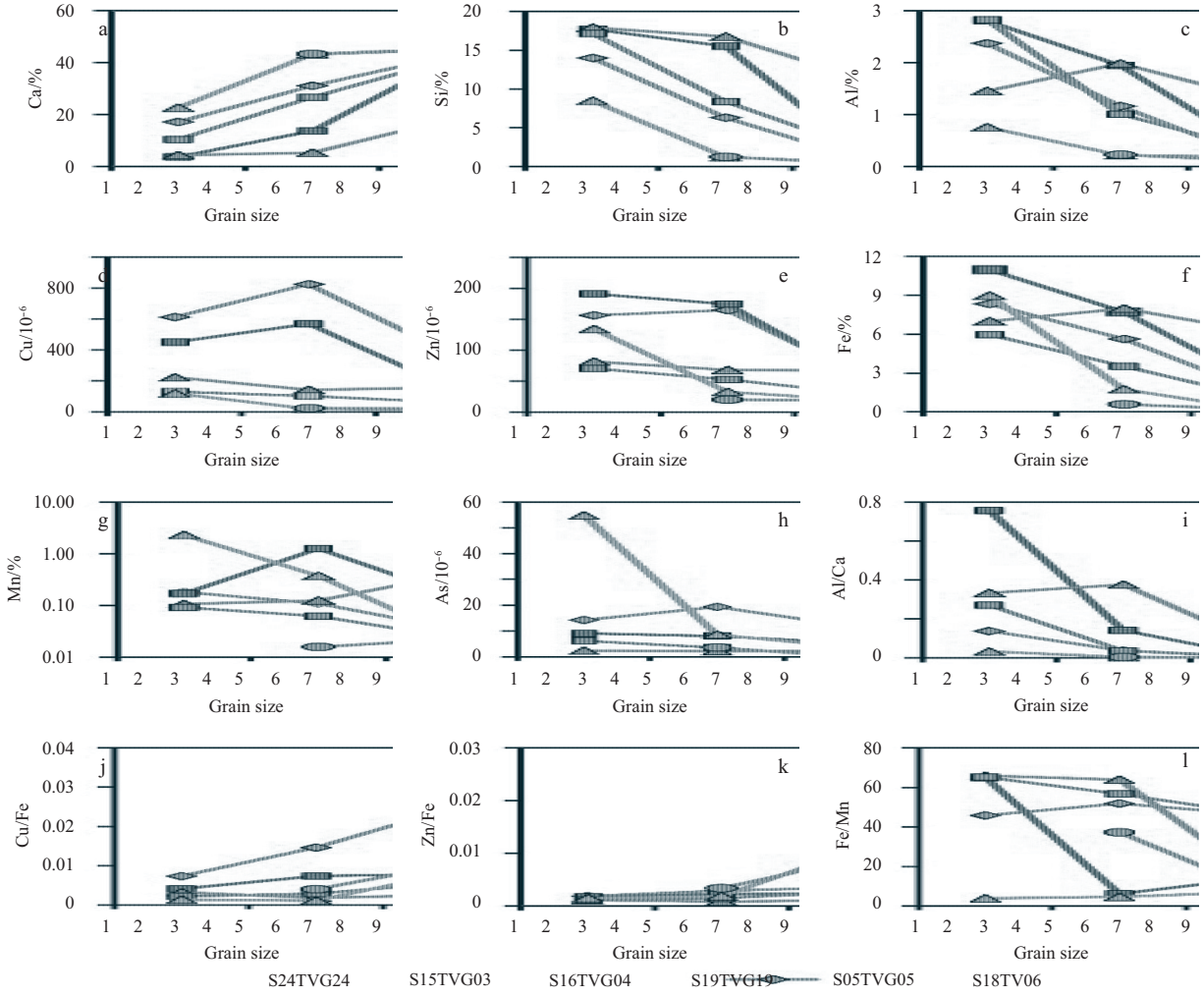

Fig. 5. Element line chart of sediments of different grain sizes, one-nine indicate size from coarser than 20 mesh to finer than 200 mesh.

of samples of different grain sizes, Cu and Zn contents of samples coarser than 40 mesh were significantly affected by debris (i.e., basalt glass). For this reason, the PXRF analysis results of samples finer than 40 mesh of the six sample stations were chosen to calculate the average values to represent the geochemical compositions of the sediments (Table 3). Results show that the two samples collected near the vent have relatively high contents of Cu, Zn, and As, which are 413×10^{-6} and 289×10^{-6} for Cu, both 71×10^{-6} for Zn, and 11×10^{-6} and 6×10^{-6} for As. These values are several times of the corresponding element contents of the sediments far from the vent, which indicates that the foraminifera shells was strongly influenced by the hydrothermal activity. Sediments from moderate distance of the vent had significantly high Fe, Mn, and Si contents, while the corresponding Cu and Zn contents were slightly lower than samples near the vent but still greater than samples far from the vent (Fig. 6a, Table 3). Element contents in the two samples far from the vent were relatively low, with Cu of 28×10^{-6} and 20×10^{-6}, Zn of 15×10^{-6} and 28×10^{-6}. However, contents of As of these samples were similar to samples collected a moderate distance from the hydrothermal vent. These results showed characteristics similar to those of the sediments from other mid-oceanic ridge hydrothermal fields (i.e., the Endeavour hydrothermal field), which are rich in Cu and Zn, whose levels decrease with increasing distance from the vent (Hrische-

Table 4. PXRF analytical data and the ratios of elements content in sediment samples

SAMPLE	Ca	Si	Al	Mo	Cu	Zn	Pb	As	Fe	Mn	Ni	Cr	Ti	Cu/Fe	Zn/Fe	Cu/Mn	Zn/Mn
S24TVG24	44.62	1.42	0.27	5	413	71	6	11	1.48	361	37	33	351	0.027 9	0.004 8	1.14	0.20
S15TVG03	41.21	2.92	0.46	7	289	71	4	6	2.49	946	47	38	539	0.011 6	0.002 9	0.31	0.08
S16TVG04	27.31	5.66	0.73	3	98	41	4	3	3.02	619	178	298	515	0.003 2	0.001 4	0.16	0.07
S19TVG19	38.26	4.78	0.73	4	86	42	4	3	1.93	615	91	175	651	0.004 4	0.002 2	0.14	0.07
S18TVG06	46.39	1.07	0.19	5	28	20	5	3	0.29	295	30	25	146	0.009 5	0.007 0	0.09	0.07
S05T VG05	46.13	0.81	0.19	5	15	28	6	3	0.22	340	40	56	163	0.006 9	0.012 6	0.04	0.08
Deep sea carbonates	31.24	3.2	2.0		50	35		1	0.9	6 700	35		770				

Note: Ca, Si, Al and Fe contents are given in percent, and other elements are in 10^{-6}. Data concerning deep ocean sediments are from Radke et al. (2011).

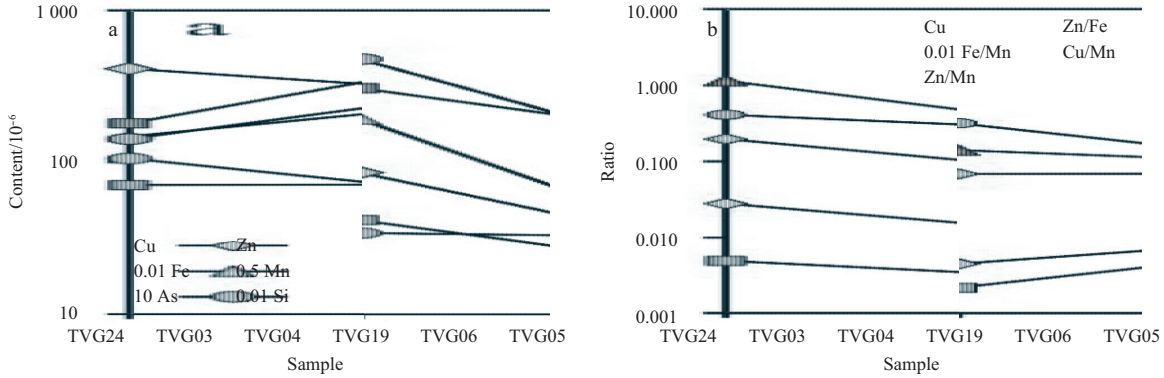

Fig. 6. Element contents of sediment samples collected different distances from hydrothermal vents.

va and Scott, 2007; Shearme et al., 1983). Thus, it can be inferred that the PXRF can indicate the ore-forming elements enrichment features of the sediments from the mid-oceanic ridges effectively, and the Cu, Zn, and As contents can be applied as indicators in the exploration for polymetallic sulfides (Radke et al., 2011).

Fe and Mn distribution features are different from Cu, Zn, and As. Samples collected moderate distances from the hydrothermal vents have higher Fe and Mn contents than sediments close to or far from the hydrothermal vent. Previous studies have indicated that Fe and Mn contents in the hydrothermal fluid of the study area were significantly higher than those of sea water, with soluble Fe consist of 50% of the whole content (Wang et al., 2012). This indicated that Fe did not precipitate rapidly after the hydrothermal fluid erupted out of the seafloor. Many previous investigations have shown that Fe and Mn can migrate far away after the fluid erupted from the seafloor, and then they became distributed around the hydrothermal vent in the form of Fe and Mn sediments (Cronan, 1983). For example, more than 35% of the Fe and almost all Mn still remain in the hydrothermal plumes in solvable forms after mixture of the hydrothermal fluid and the sea water (Mottl and Mcconachy, 1990); Edmonds and German (2004) found that ferric oxide particles in the plumes of the Rainbow hydrothermal fluid field located on the Mid-Atlantic Ridge could spread up to 10 km along the direction of the oceanic current. Sulfide particles in the hydrothermal plumes are continuously oxidized as the plumes spread, which further lowers the Cu and Zn content in the plume (Feely et al., 1992; German and Sparks, 1993). This produces relatively high Fe/Mn ratios and high levels of Cu, Zn, and Fe in sediments near the vent (German et al., 1999), and sediments far from the vent have relatively high Mn content and Mn/Fe ratios (Rowe et al., 2004). As a result, the concentrations of Fe and Mn and the ratios of Fe, Mn vs Cu, and Zn can be used as trace indicators for hydrothermal vent. For instance, the Cu/Fe ratio in the sediments near the TAG hydrothermal field and the OBS hydrothermal field were 0.090 and 0.71, respectively, and the corresponding Zn/Fe ratios were 0.006 and 0.037, respectively (German et al., 1993), which were profoundly higher than in the pelagic background sediment (BRT).

The results of this paper further indicate that although Cu/Fe and Zn/Fe ratios in the sediments near the vent were higher, sediments collected moderate distances from the hydrothermal field showed higher Fe and Mn contents than sediments near the hydrothermal field, leading to lower Cu/Fe and Zn/Fe ratios than samples far from the vent. In this way, it is difficult to determine the location or the direction of the hydrothermal vent in uninvestigated areas by Fe and Mn contents alone or by Cu/Fe and Zn/Fe ratios alone, especially when there were only a few sampling stations. Results here indicated that the Cu/Mn and Zn/Mn ratios were significantly higher in samples collected near the vent (TVG24 and TVG03) than in those collected a moderate distance from the vent (TVG04 and TVG19) (Fig. 6b), indicating that Cu/Mn and Zn/Mn ratios may also be indicators suitable for use in sulfide exploration.

5.3 *Zoning of elements*

A huge number of investigations on the mitigation and zoning of elements near hydrothermal vents have been performed. It has been reported that the contents of the ore-forming elements in the plumes are several times higher than sea water (Sands et al., 2012). Copper and zinc sulfides usually precipitate rapidly after the hydrothermal fluid eruption from the seafloor, and form sulfide sediments around the vent in short distances (German et al., 1991). Fe and Mn migrate long distance within the hydrothermal fluid, and then distributed in sediments around the hydrothermal vent (Cronan, 1983). In this study, analysis of the six sediment samples from the Southwest Indian Ridge showed the element contents of Cu, Zn, and As to be relatively high in the sediments close to the vent, and sediments with a moderate distance from the hydrothermal area showed higher Fe and Mn contents. Therefore, for sediments near the hydrothermal vent, Cu, Zn, and As are the elements in the inner zone, while Fe and Mn are the elements in the outer zone.

Further, analytical data of this study from six sediment samples with various grain sizes from different sampling stations indicated that the two samples near the vent had higher Cu/Fe ratios than other samples (Fig. 7), which is consistent with the findings that the ratio of element/Fe decreased as the overall Fe content of the neutral plumes decreased (Edmonds and German, 2004). Relationships between Zn, As, and Fe are similar to those between Zn, As, and Cu, indicating that the two samples rich in Zn and As also have relatively high Zn/Fe and As/Fe ratios. However, the degree of reduction of the Cu/Fe ratio was far more pronounced than that of the Zn/Fe ratio, while the degree of reduction of the Zn/Fe ratio was significantly higher than that of As/Fe, indicating that the precipitation speed of Cu was faster than that of Zn and the precipitation speed of Zn was faster than that of As, in accordance with the precipitation order of the elements near the hydrothermal vent reported by Mottl and Mcconachy (1990). Here, the order of precipitation and zoning of the elements near the hydrothermal vent was found to be as follows: Cu, Zn, As, Fe, and Mn.

6 Conclusions

(1) Sediments coarser than 20 mesh in the Southwest Indian

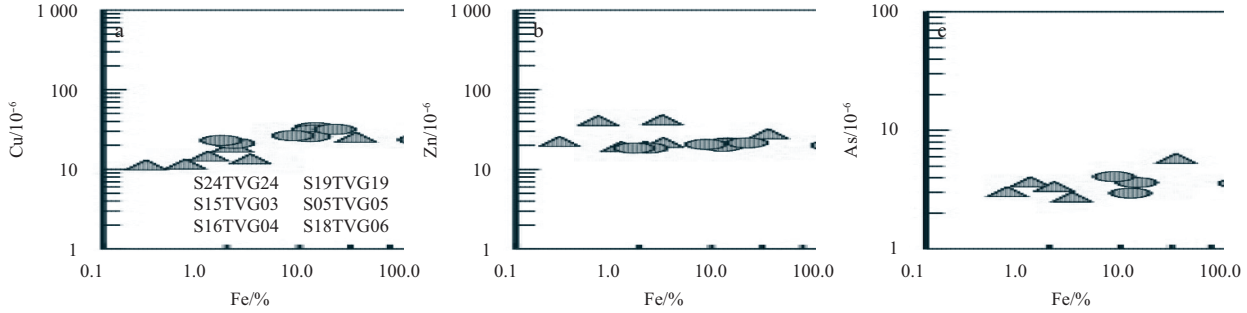

Fig. 7. Scatter graph of elements contents in sediment samples.

Ridge mainly contained rock debris and basaltic glass; sediments of 20–40 mesh still consisted primarily of rock debris and basaltic glass, but there was more coarse foraminifera sand; sediments finer than 40 mesh consisted mainly of foraminifera sand, which represents typical pelagic sediments.

(2) Contents of the elements Cu, Zn, Fe, and Mn were relatively constant in sediments finer than 40 mesh, but higher in coarser samples, probably from basaltic debris and glass component in these sediments. Thus, sediments finer than 40 mesh should be used as analytical samples during the geochemical exploration of hydrothermal vent at mid-oceanic ridges.

(3) Contents of the elements Cu, Zn, and As were relatively high in sediments near the vent, and sediments collected a moderate distance from the hydrothermal field had higher Fe and Mn contents. For sediments near or far from the vent, the ratios of Cu/Fe and Zn/Fe were higher than sediments collected a moderate distance away. As distance increased, the ratios of Cu/Mn and Zn/Mn decreased significantly. Sediments showed elements zoning of Cu, Zn, As, Fe, and Mn around the hydrothermal vent.

(4) Ore-forming elements enrichment features in the calcareous sediments of the mid-ocean ridges can be determined effectively using PXRF. Element contents of Cu, Zn, As, Fe, and Mn and their ratios can be used as indicators in the geochemical exploration for polymetallic sulfides. This method satisfies the requirements of rapidly identifying geochemical anomalies in the sediments from the mid-oceanic ridges.

Acknowledgements

All samples in this study were collected during Leg 2 of the 34th cruise on R/V *Dayangyihao*. We greatly appreciate the contributions by all the researchers on board.

References

Aitchison J. 1986. The Statistical Analysis of Compositional Data. London: Chapman & Hall

Arne D C, Mackie R A, Jones S A. 2014. The use of property-scale portable X-ray fluorescence data in gold exploration: advantages and limitations. Geochemistry: Exploration, Environment, Analysis, 14(3): 233–244

Bloemsma M R, Zabel M, Stuut J B W, et al. 2012. Modelling the joint variability of grain size and chemical composition in sediments. Sedimentary Geology, 280: 135–148

Chen Yuanyuan, Yu Bingsong, Su Xin, et al. 2013. Mineralogical and geochemical characteristics of the calcareous sediments in southwest Indian ridge. Geological Science and Technology Information (in Chinese), 32(1): 107–113

Cronan D S. 1983. Metalliferous sediments in the CCOP/SOPAC region of the southwest Pacific: with particular reference to geochemical exploration for the deposits. UN ESCAP, CCOP/SOPAC Technical Bulletin no. 4: 55

Dick H J B, Lin Jian, Schouten H. 2003. An ultraslow-spreading class of ocean ridge. Nature, 426(6965): 405–412

Edmonds H N, German C R. 2004. Particle geochemistry in the Rainbow hydrothermal plume, Mid-Atlantic Ridge. Geochimica et Cosmochimica Acta, 68(4): 759–772

Feely R A, Lewison M, Massoth G J, et al. 1987. Composition and dissolution of black smoker particulates from active vents on the Juan de Fuca Ridge. Journal of Geophysical Research, 92(B11): 11347–11363

Feely R A, Massoth G J, Baker E T, et al. 1992. Tracking the dispersal of hydrothermal plumes from the Juan de Fuca Ridge using suspended matter compositions. Journal of Geophysical Research, 97(B3): 3457–3468

Fisher L, Gazley M F, Baensch A, et al. 2014. Resolution of geochemical and lithostratigraphic complexity: a workflow for application of portable X-ray fluorescence to mineral exploration. Geochemistry: Exploration, Environment, Analysis, 14(2): 149–159

Gazley M F, Tutt C M, Brisbout L I, et al. 2014. Application of portable X-ray fluorescence analysis to characterize dolerite dykes at the Plutonic Gold Mine, Western Australia. Geochemistry: Exploration, Environment, Analysis, 14(3): 223–231

Georgen J E, Lin Jian, Dick H J B. 2001. Evidence from gravity anomalies for interactions of the Marion and Bouvet hotspots with the Southwest Indian Ridge: effects of transform offsets. Earth and Planetary Science Letters, 187(3–4): 283–300

German C R. 2003. Hydrothermal activity on the eastern SWIR (50°-70°E): evidence from core-top geochemistry, 1887 and 1998. Geochemistry, Geophysics, Geosystems, 4(7): 9102

German C R, Campbell A C, Edmond J M. 1991. Hydrothermal scavenging at the Mid-Atlantic Ridge: modification of trace element dissolved fluxes. Earth and Planetary Science Letters, 107(1): 101–114

German C R, Hergt J, Palmer M R, et al. 1999. Geochemistry of a hydrothermal sediment core from the OBS vent-field, 21°N East Pacific Rise. Chemical Geology, 155(1–2): 65–75

German C R, Higgs N C, Thomson J, et al. 1993. A geochemical study of metalliferous sediment from the TAG Hydrothermal Mound, 26°08′N, Mid-Atlantic Ridge. Journal of Geophysical Research, 98(B6): 9683–9692

German C R, Sparks R S J. 1993. Particle recycling in the TAG hydrothermal plume. Earth and Planetary Science Letters, 116(1–4): 129–134

Graham I J, Glasby G P, Churchman G J. 1997. Provenance of the detrital component of deep-sea sediments from the SW Pacific Ocean based on mineralogy, geochemistry and Sr isotopic composition. Marine Geology, 140(1–2): 75–96

Hall G E M, Bonham-Carter G F, Buchar A. 2014. Evaluation of portable X-ray fluorescence (pXRF) in exploration and mining: Phase 1, control reference materials. Geochemistry: Exploration, Environment, Analysis, 14(2): 99–123

Han Xiqiu, Wu Guanghai, Cui Ruyong, et al. 2010. Discovery of a hydrothermal sulfide deposit on the Southwest Indian Ridge at 49.2°E. In: 2010 Fall Meeting. San Francisco: American Geophysical Union

Han Zongzhu, Zhang He, Fan Dejiang, et al. 2012. The characteristic of geochemistry and genesis for mafic and Utrlmafic rocks from the 50 °E of Southwest Indian Ridge. Periodical of Ocean Uni-

versity of China (in Chinese), 42(9): 69–76
Hannington M, Jamieson J, Monecke T, et al. 2011. The abundance of seafloor massive sulfide deposits. Geology, 39(12): 1155–1158
Herzig P M, Hannington M D. 1995. Polymetallic massive sulfides at the modern seafloor: a review. Ore Geology Reviews, 10(2): 95–115
Hou Xiandeng, He Yihua, Jones B T. 2004. Recent advances in portable X-ray fluorescence spectrometry. Applied Spectroscopy Reviews, 39(1): 1–25
Hrischeva E, Scott S D. 2007. Geochemistry and morphology of metalliferous sediments and oxyhydroxides from the Endeavour segment, Juan de Fuca Ridge. Geochimica et Cosmochimica Acta, 71(14): 3476–3497
Huang Dasong, Zhang Xiaoyu, Zhang Guoyin, et al. 2016. Geochemical characteristics of sediments in Southwest Indian Ridge 48.6°–51.7°E. Geological Science and Technology Information (in Chinese), 35(1): 22–29
Keays R R, Scott R B. 1976. Precious metals in ocean-ridge basalts; implications for basalts as source rocks for gold mineralization. Economic Geology, 71(4): 705–720
Kenna T C, Nitsche F O, Herron M M, et al. 2011. Evaluation and calibration of a field portable X-ray fluorescence spectrometer for quantitative analysis of siliciclastic soils and sediments. Journal of Analytical Atomic Spectrometry, 26(2): 395–405
Li Zhenggang, Chu Fengyou, Jin Lu, et al. 2016. Major and trace element composition of surface sediments from the Southwest Indian Ridge: evidence for the incorporation of a hydrothermal component. Acta Oceanologica Sinica, 35(2): 101–108
Liao Guanghong, Zhou Beifeng, Liang Chujin, et al. 2016. Moored observation of abyssal flow and temperature near a hydrothermal vent on the Southwest Indian Ridge. Journal of Geophysical Research, 121(1): 836–860
Lisitzin A P, Lukashin V N, Gordeev V V, et al. 1997. Hydrological and geochemical anomalies associated with hydrothermal activity in SW Pacific marginal and back-arc basins. Marine Geology, 142(1–4): 7–45
Mäkinen E, Korhonen M, Viskari E L, et al. 2006. Comparison of XRF and FAAS methods in analysing CCA contaminated soils. Water, Air, & Soil Pollution, 171(1–4): 95–110
Marchig V, Gundlach H, Möller P, et al. 1982. Some geochemical indicators for discrimination between diagenetic and hydrothermal metalliferous sediments. Marine Geology, 50(3): 241–256
Meinhardt A K, März C, Stein R, et al. 2014. Regional variations in sediment geochemistry on a transect across the Mendeleev Ridge (Arctic Ocean). Chemical Geology, 369: 1–11
Melquiades F L, Appoloni C R. 2004. Application of XRF and field portable XRF for environmental analysis. Journal of Radioanalytical and Nuclear Chemistry, 262(2): 533–541
Mottl M J, McConachy T F. 1990. Chemical processes in buoyant hydrothermal plumes on the East Pacific Rise near 21°N. Geochimica et Cosmochimica Acta, 54(7): 1911–1927
Nakamura K, Kato Y, Tamaki K, et al. 2007. Geochemistry of hydrothermally altered basaltic rocks from the Southwest Indian Ridge near the Rodriguez triple junction. Marine Geology, 239(3–4): 125–141
Palma C, Oliveira A, Valença M, et al. 2013. Major and minor element geochemistry of deep-sea sediments in the Azores Platform and southern seamount region. Marine Pollution Bulletin, 75(1–2): 264–275
Piercey S J, Devine M C. 2014. Analysis of powdered reference materials and known samples with a benchtop, field portable X-ray fluorescence (pXRF) spectrometer: evaluation of performance and potential applications for exploration lithogeochemistry. Geochemistry: Exploration, Environment, Analysis, 14(2): 139–148
Piorek S. 1997. Field-portable X-ray fluorescence spectrometry: past, present, and future. Field Analytical Chemistry & Technology, 1(6): 317–329
Radke L C, Heap A D, Douglas G, et al. 2011. A geochemical characterisation of deep-sea floor sediments of the northern Lord Howe Rise. Deep Sea Research II, 58(7–8): 909–921
Rona P A. 1984. Hydrothermal mineralization at seafloor spreading centers. Earth-Science Reviews, 20(1): 1–104
Ross P S, Bourke A, Fresia B. 2014. Improving lithological discrimination in exploration drill-cores using portable X-ray fluorescence measurements: (1) Testing threes Olympus Innov-X analysers on unprepared cores. Geochemistry: Exploration, Environment, Analysis, 14(2): 171–185
Rowe A J, Wilkinson J J, Coles B J, et al. 2004. Chicxulub: testing for post-impact hydrothermal input into the Tertiary ocean. Meteoritics & Planetary Science, 39(7): 1223–1231
Rusakov V Y, Shilov V V, Ryzhenko B N, et al. 2013. Mineralogical and geochemical zoning of sediments at the Semenov cluster of hydrothermal fields, 13°31′–13°30′N, Mid-Atlantic Ridge. Geochemistry International, 51(8): 646–669
Sands C M, Connelly D P, Statham P J, et al. 2012. Size fractionation of trace metals in the Edmond hydrothermal plume, Central Indian Ocean. Earth and Planetary Science Letters, 319–320: 15–22
Sauter D, Cannat M, Meyzen C, et al. 2009. Propagation of a melting anomaly along the ultraslow Southwest Indian Ridge between 46°E and 52°20′E: interaction with the Crozet hotspot?. Geophysical Journal International, 179(2): 687–699
Sauter D, Patriat P, Rommevaux-Jestin C, et al. 2001. The Southwest Indian Ridge between 49°15′E and 57°E: focused accretion and magma redistribution. Earth and Planetary Science Letters, 192(3): 303–317
Shearme S, Cronan D S, Rona P A. 1983. Geochemistry of sediments from the TAG Hydrothermal Field, M.A.R. at latitude 26°N. Marine Geology, 51(3–4): 269–291
Tao Chunhui, Li Huaiming, Huang Wei, et al. 2011. Mineralogical and geochemical features of sulfide chimneys from the 49°39′E hydrothermal field on the Southwest Indian Ridge and their geological inferences. Chinese Science Bulletin, 56(26): 2828–2838
Tao Chunhui, Li Huaiming, Jin Xiaobing, et al. 2014. Seafloor hydrothermal activity and polymetallic sulfide exploration on the Southwest Indian Ridge. Chinese Science Bulletin, 59(19): 2266–2276
Tao Chunhui, Lin Jian, Guo Shiqin, et al. 2012. First active hydrothermal vents on an ultraslow-spreading center: southwest Indian Ridge. Geology, 40(1): 47–50
Wang Wei, Chu Fengyou, Zhu Jihao, et al. 2013. Mantle melting beneath the Southwest Indian Ridge: signals from clinopyroxene in abyssal peridotites. Acta Oceanologica Sinica, 32(12): 50–59
Wang Zhenbo, Wu Guanghai, Han Chenhua. 2014. Geochemical characteristics of hydrothermal deposits and basalts at 49.6°E on the Southwest Indian Ridge. Journal of Marine Sciences (in Chinese), 32(1): 64–73
Wang Hu, Yang Qunhui, Ji Fuwu, et al. 2012. The geochemical characteristics and Fe(II) oxidation kinetics of hydrothermal plumes at the Southwest Indian Ridge. Marine Chemistry, 134–135: 29–35
Wu C M, Tsai H T, Yang K H, et al. 2012. How reliable is X-ray fluorescence (XRF) measurement for different metals in soil contamination?. Environmental Forensics, 13(2): 110–121
Xia Qinglin, Cheng Qiuming, Lu Jianpei, et al. 2011. Application of portable XRF technology to identification of mineralization and alteration along drill in the Nihe iron deposit, Anhui, East China. Earth Science-Journal of China University of Geosciences (in Chinese), 36(2): 336–340
Yang Yaomin, Ye Jun, Shi Xuefa, et al. 2011. Mineralogy and geochemistry of submarine metalliferous sediments and significances for hydrothermal activity. Journal of Central South University: Science and Technology (in Chinese), 42(S2): 65–74
Yuan Zhaoxian, Cheng Qiuming, Xia Qinglin, et al. 2014. Spatial patterns of geochemical elements measured on rock surfaces by portable X-ray fluorescence: application to hand specimens and rock outcrops. Geochemistry: Exploration, Environment, Analysis, 14(3): 265–276
Zhou Huaiyang, Dick H J B. 2013. Thin crust as evidence for depleted mantle supporting the Marion Rise. Nature, 494(7436): 195–200